International Journal of Remote Sensing
Vol. 27, No. 10, 20 May 2006, 2077–2085

Taylor & Francis
Taylor & Francis Group

An automatic atmospheric correction algorithm for visible/NIR imagery

R. RICHTER*†, D. SCHLÄPFER‡ and A. MÜLLER†
†DLR, German Aerospace Center, Remote Sensing Data Center, D-82234 Wessling, Germany
‡University of Zurich, Remote Sensing Laboratories, Winterthurerstr. 190, CH-8057-Zurich, Switzerland

(*Received 4 July 2005; in final form 15 November 2005*)

The automatic correction of atmospheric effects currently requires visible to short-wave spectral bands (400–2500 nm) to derive high accuracy surface reflectance data. Common techniques employ spectral correlations of dark targets in the short-wave infrared (SWIR, around 2.2 μm), blue (480 nm) and red (660 nm) regions to derive the aerosol optical depth. A large number of current Earth-observing satellite sensors have only three or four spectral channels in the visible and near-infrared (VNIR) region (400–1000 nm), making an automatic image-based atmospheric correction very difficult. This contribution presents a new algorithm and first results with VNIR imagery. The method starts with the assumption of average clear atmospheric conditions (aerosol optical depth AOD=0.27, corresponding to a visibility of 23 km) and calculates the surface reflectance in the red and near-infrared (NIR) bands. The second step derives a mask of dark vegetation pixels. It is calculated using multiple thresholds of vegetation index combined with red and NIR surface reflectance values. Then the red band surface reflectance for the dark pixels is estimated from the NIR reflectance as $\rho_{red}=0.1\ \rho_{nir}$, from which the aerosol optical depth (or visibility) can be calculated. The core of the VNIR algorithm consists of two subsequent iteration loops (visibility and ρ_{red}) to improve the visibility estimate.

Results of the VNIR method are presented for Landsat-5 Thematic Mapper (TM) and Landsat-7 Enhanced Thematic Mapper Plus (ETM+) imagery using only the first four bands. The performance of the method is compared to the established dark pixel technique where the SWIR bands are included. Results show that the deviation between both methods is usually less than 0.005 reflectance units if measured in terms of the scene-average reflectance, indicating a useful potential for this approach.

1. Introduction

Surface reflectance data obtained after atmospheric correction of satellite sensor imagery offers some advantages compared with the usage of the original digital number (DN) or calibrated radiance data: (i) the interpretation of surface reflectance spectra is easier than the interpretation of DN spectra, which depend on atmospheric conditions and the solar illumination geometry, (ii) surface reflectance spectra can be compared with library or field spectra, (iii) to compare

*Corresponding author. Email: rudolf.richter@dlr.de

International Journal of Remote Sensing
ISSN 0143-1161 print/ISSN 1366-5901 online
http://www.tandf.co.uk/journals
DOI: 10.1080/01431160500486690

and increase the scope of multi-sensor imagery, data must be calibrated to physical units (e.g. reflectance) as provided after atmospheric correction, and (iv) the atmospheric scattering acts as a spatial low-pass filter causing a certain degree of blurring, which can be removed or at least strongly diminished with atmospheric correction (Kaufman 1985, Richter 1996).

While imaging spectrometers have the potential to calculate the most important atmospheric parameters (aerosol optical depth or visibility, water vapour column) from the scene (Kaufman *et al*. 1997, Schläpfer *et al*. 1998, Bojinski *et al*. 2004) some compromises obviously have to be made during the automatic processing of multispectral visible and near-infrared (VNIR) data with typically three or four bands, e.g. Ikonos, Quickbird, Orbview, DMC (Disaster Monitoring Constellation), historic Landsat MSS (Multispectral Scanner) or SPOT-1 to SPOT-3 (Système Probatoire d'Observation de la Terre) data.

Dense dark vegetation (DDV) has been identified as a suitable reference to derive the aerosol optical depth over land surfaces (Kaufman and Sendra 1988, Kaufman *et al*. 1997). The method is based on a stable relationship between surface reflectance ρ in the short-wave infrared (SWIR; 2100–2200 nm) and reflectance in the blue (480 nm) and red (660 nm) wavelengths. It starts with the approximation $\rho_{\mathrm{swir}} = \rho_{\mathrm{swir}}^{\mathrm{TOA}}$ where ρ^{TOA} is the top-of-atmosphere reflectance. This approximation is fairly accurate, because of the small path radiance and high atmospheric transmittance $\tau > 0.9$ in the SWIR region (compare figure 1, which contains the atmospheric transmittance with the absorption and window regions and a typical conifer reflectance spectrum). Then, the relationships $\rho_{\mathrm{blue}} = \rho_{\mathrm{swir}}/4$ and $\rho_{\mathrm{red}} = \rho_{\mathrm{swir}}/2$ are employed and the differences between the TOA apparent reflectance and the reflectance from the above relationships are used to calculate the path radiance and corresponding aerosol optical depth. The spectral reflectance correlation between the red and SWIR wavelengths is sufficiently stable for an aerosol retrieval. This contribution investigates the possibility to perform an automatic atmospheric correction exploiting the red and NIR correlation for VNIR sensors.

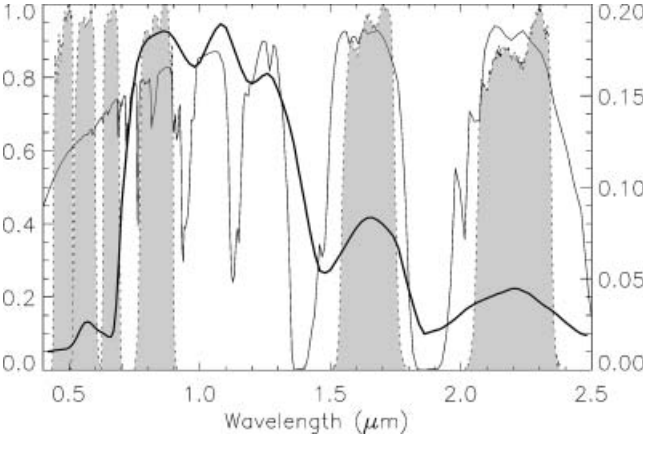

Figure 1. Atmospheric transmittance (thin line, left y axis) and coniferous reflectance spectrum (thick line, right y axis). The shaded areas mark the relative spectral response functions of ETM+.

2. VNIR atmospheric correction method

The proposed automatic correction method for broad-band multispectral VNIR sensors, typically with three spectral bands (green, red, NIR) or four bands (additional blue band) employs the following approximations:

1. Water vapour column: since it cannot be estimated from the image data, either a seasonal climatological value (summer, winter, location-dependent) is taken or measurements are taken from meteorological stations in the corresponding area.
2. Ozone absorption: again a seasonal geography-dependent value has to be used. The typical elevation-dependence of ozone concentration as implemented in the MODTRAN code (Berk *et al.* 2003) is taken into account.
3. Aerosol type (single scattering albedo, phase function): if a blue and red band are available the aerosol type can be estimated (Kaufman *et al.* 1997), otherwise it has to be selected from the climatology of the area where the scene was acquired using built-in MODTRAN aerosols (e.g. rural, urban, maritime).

The other main absorbing gases (CO_2, O_2) are taken into account, however their variation on a global scale is small and they play a minor role for broad-band VNIR sensors. The contribution of molecular scattering is known and depends only on pressure level or elevation. The remaining most important atmospheric parameter that varies in space and time is the aerosol optical depth or corresponding meteorological range (shortly named visibility).

To account for the pressure dependence of the molecular scattering and the height profiles of the absorbing gases the average elevation of the scene has to be specified, or in case of a mountainous terrain an appropriate digital elevation model should be included (Richter 1998).

The difference between the approach presented here and the VNIR approach of Kaufman and Sendra (1988) is that the 1988 algorithm works with a constant *a priori* reflectance in the red band (e.g. $\rho = 0.02$) while the proposed method uses a variable reflectance that depends on the vegetation index and the NIR reflectance. The second difference is that the mask of the reference pixels is not obtained employing two fractions (f_1 = thresholded NDVI, and f_2 = lowest radiance in NIR) based on *a priori* knowledge of vegetation in the scene, but with the multiple threshold criterion given below. This benefit over the previous model is the basis for a modified DDV algorithm tailored to VNIR sensors.

The method employs iterations with three visibilities (10, 23, 60 km) to cover a large range of aerosol loadings. It starts with the assumption of average clear atmospheric conditions (aerosol optical depth AOD = 0.27 at 550 nm, corresponding to a visibility of 23 km, see figure 2) and calculates the surface reflectance in the red and NIR bands employing look-up tables (Richter 1996, 1998) based on the MODTRAN radiative transfer code (Berk *et al.* 2003).

The method continues with two iterations of visibility 60 km and 10 km. The order in which the visibilities are used is not important, because a failure to identify DDV reference pixels at the first visibility is independent of the results of the second visibility. The next step derives a mask of DDV pixels using the ratio vegetation index (RVI) of the red and near-infrared surface reflectance, $\mathrm{RVI} = \rho_{\mathrm{nir}}/\rho_{\mathrm{red}}$ and

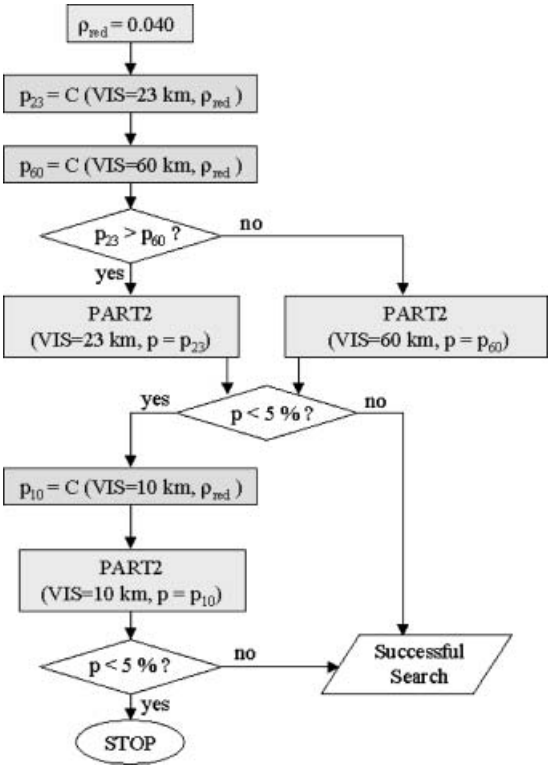

Figure 2. Flow chart of the automatic atmospheric correction for VNIR sensors.

multiple reflectance thresholds:

$$\text{The masked DDV pixels have to fulfil : RVI} \geq 3 \text{ and } 0.10 \leq \rho_{\text{nir}} \leq 0.25 \text{ and } \rho_{\text{red}} \leq 0.04.$$

Instead of the RVI criterion one could also use a normalized difference vegetation index criterion (e.g. NDVI$\geqslant$0.5) to identify vegetation. The condition $0.10 \leqslant \rho_{\text{nir}}$ excludes clear and turbid water as well as mixed coniferous-soil pixels with a large percentage of dark soil or shadow background, $\rho_{\text{nir}} \leqslant 0.25$ excludes bright vegetation (e.g. meadows, deciduous forests), and the last criterion is a start threshold for the red band that is iterated as explained below. Soil pixels are excluded with the combination of all four conditions.

The calculation of the mask of DDV reference pixels is based on surface reflectance, which implies it depends on the start visibility of VIS=23 km (AOD=0.27) which is appropriate for situations of clear atmospheric conditions (VIS=15–40 km). The output of the mask criterion is a percentage p of reference pixels with respect to the total number of scene pixels which must exceed 5% for a successful search. Besides the NIR reflectance thresholds that are kept constant here, this percentage also depends on the start threshold $\rho_{\text{red}} \leqslant 0.04$, so this functional behaviour is indicated by the following equation

$$p = C(\text{VIS}, \rho_{\text{red}}) \tag{1}$$

where C indicates the multiple threshold criterion defined above.

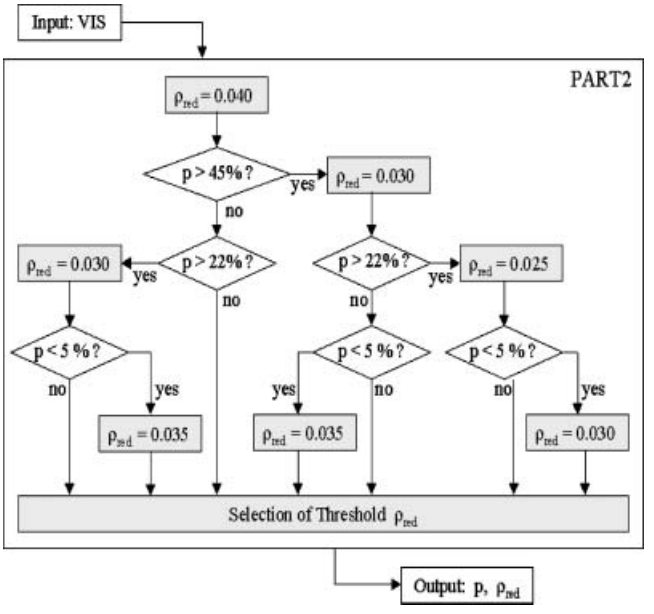

Figure 3. Flow chart of the masking of reference pixels.

Figure 2 shows the overall algorithm with the visibility iterations, the blocks with 'PART2' indicate the second iteration with the surface reflectance ρ_{red} as detailed in figure 3. If the percentage of DDV reference pixels is smaller than 5% of the scene the search for reference pixels is iterated. The first iteration employs VIS=60 km (AOD=0.13) to check the possibility of very clear atmospheric conditions (range VIS=40–100 km). Again, if the percentage is smaller than 5%, the search is iterated with VIS=10 km (AOD=0.80) to account for a much larger aerosol content (range VIS=9–15 km). If more than 5% reference areas are found for VIS=23 km (percentage p_{23}) and for VIS=60 km (p_{60}) then the criterion with the larger percentage is taken and the ρ_{red} iteration (in 'PART2', figure 3) is executed. The algorithm terminates if less than 5% reference pixels are found after these visibility and ρ_{red} iterations.

If a large number of DDV reference pixels is found (percentage $p>45\%$) then ρ_{red} is tentatively decreased to 0.03, and if the percentage is still higher than 22% further down to 0.025 (see figure 3) to consider only the darkest pixels available. The strategy is to reduce the threshold ρ_{red} down to 0.025 as long as the percentage of reference areas is greater than 5%. The large start value of $\rho_{red}=0.04$ provides a certain safety margin in order not to miss dark pixels, which could be caused by slight radiometric calibration errors in the red band, inaccuracies of the radiative transfer code, or because of the discrete set of visibility values. In addition, surfaces with less than 100% dark vegetation cover would be included in the mask of reference pixels.

The third step calculates the surface reflectance in the red band as a fraction α of the NIR band reflectance for the masked DDV pixels:

$$\rho_{red} = \alpha\rho_{nir} = 0.1\rho_{nir} \quad (2)$$

As an independent validation of the new method, the corresponding equation for

sensors with SWIR bands is used (Kaufman *et al.* 1997)

$$\rho_{red} = \beta \rho_{swir} \tag{3}$$

where β=0.5 for a 2.2 μm band (SWIR2), and β=0.25 for a 1.6 μm band (SWIR1).

In this study the SWIR DDV pixels were masked with the criterion ρ_{swir2}=0.05 and ρ_{swir1}=0.10 with the additional threshold NDVI$\geq$0.1, which excluded water surfaces. Similar to the empirical SWIR relationships the coefficient α=0.1 is an average empirical value yielding results in close agreement with the SWIR method as shown in the next section. However, deviations from the nominal value α=0.1 can vary about 30% depending on biome, which will be the subject of a separate paper.

In principle, equation (2) could also be used with an offset term, i.e. $p_{red}=\alpha_0+\alpha_1\rho_{nir}$, but the following results were obtained with an offset α_0=0. All the thresholds in the definition of this algorithm were also tested for other sensors, e.g. SPOT-3, DMC, Ikonos, and worked well. Before the final step of atmospheric correction takes place the visibility of non-reference pixels in the scene can be set to the average value of the reference pixels or a spatial interpolation can be applied. For a statistical evaluation both options (without and with interpolation) yield very similar results, and the first one is used in this study.

3. Results and discussion

This section shows selected results of the proposed VNIR correction method. Up to now it was applied to 20 scenes with a range of solar geometries (solar zenith angles from 24° to 59°), atmospheric conditions (visibility 10–90 km corresponding to AOD=0.80–0.10 at 550 nm), and ground elevations (sea level to 2.5 km above sea level). Only scenes with at least 5% dark reference pixels were employed in this study, but most of these scenes contained 10% or more of the reference areas. Landsat-5 Thematic Mapper (TM) and Landsat-7 ETM+ (Enhanced Thematic Mapper Plus) datasets were taken for the assessment of the VNIR algorithm. The VNIR technique was applied using only Landsat bands 1–4, and a comparison was made to the results of the SWIR2 method (Kaufman *et al.* 1997) where all six reflective bands were taken. The well established SWIR2 method was applied with the standard regression coefficient of β=0.5 in equation (3) for all biomes, and the VNIR with the standard coefficient α=0.1. The SWIR2 results serve as the reference case against which the VNIR results are compared.

Table 1 presents seven scenes of Landsat-5 TM and Landsat-7 ETM+ and the derived average scene visibility and the difference in aerosol optical depth between both methods ΔAOD=AOD(SWIR2) – AOD(VNIR). Figure 4 contains the average surface reflectance results ($\bar{\rho}$) for all seven scenes.

Results obtained with the VNIR method usually deviate less than 0.5% reflectance from the SWIR method. Despite a rather large deviation in AOD of –0.088 for scene 7, the average reflectance values of both approaches agree within $\pm$0.2% reflectance for all bands (see figure 4, curve 7). The reason is that this scene contains only a percentage p=6% of reference vegetation, and mostly soil areas with somewhat higher reflectance values in the visible bands, which reduces the sensitivity to errors in the aerosol optical depth.

Occasional cases with ΔAOD=0 still yield slightly different average scene surface reflectance values, because the number and spatial distribution of the reference pixels usually is not identical for both algorithms. The differences $\Delta\rho=\bar{\rho}_{swir2}-\bar{\rho}_{vnir}$

Table 1. Summary of selected seven scenes. VIS is the visibility calculated with the VNIR method, ΔAOD is the difference of the aerosol optical depths obtained with the SWIR2 and VNIR method. The first two scenes are Landsat-5 TM data, the remainder are Landsat-7 ETM+.

Scene	Sensor	Date	Path/row	SZA (°)	VIS (km)	ΔAOD
1	TM	20 Aug. 1989	197/24	43.0	15	+0.011
2	TM	13 Aug. 1985	195/26	40.0	27	−0.043
3	ETM+	11 Sept. 1999	195/27	45.8	25	+0.066
4	ETM+	24 Aug. 2000	14/20	48.3	42	−0.086
5	ETM+	11 Aug. 2001	46/25	39.1	69	−0.021
6	ETM+	5 Oct. 2001	47/25	57.2	87	0.0
7	ETM+	8 May 2003	27/46	24.9	20	−0.088

SZA, solar zenith angle.

are especially small for high visibilities, in the example of scene 6 we obtain $\Delta\rho<0.04\%$ reflectance (see figure 4, curve 6).

The scene average surface reflectances in bands 1–3 are below 10% for the selected seven scenes. However, both methods were also compared for some surfaces of higher reflectance levels (15–30%); here the deviation was generally smaller than 0.6%. At first glance the results seem to indicate a smaller deviation of the new method for clear atmospheric conditions (scenes 5 and 6). However, this is not generally the case, since the deviation ΔAOD for scene 1 (with the lowest visibility of 15 km) is also very small. On the other hand, a large deviation ΔAOD also exists for the clear scene 4, which could be caused by a geography and biome-dependence of the coefficient α of equation (2). A larger data pool has to be processed and investigated in the future to answer these points. Future activities should also include field measurements collected with the scenes.

Table 2 summarizes the differences in calculated AODs with an AOD root mean square (RMS) error of 0.056 for the VNIR method (index 'vnir'). The evaluation of all 20 processed scenes yields a corresponding RMS error of 0.054.

It is also interesting to compare the performance of the VNIR band correlation method with the SWIR1 method (i.e. using equation (3) with $\beta=0.25$). The reason is that a logical step of a sensor enhancement is the addition of a 1.6 μm band as demonstrated by the development from SPOT-3 to SPOT-4 or from IRS-1B LISS-2 to IRS-1C LISS-3 (Kalyanaraman *et al.* 1995). In addition, the performance of the

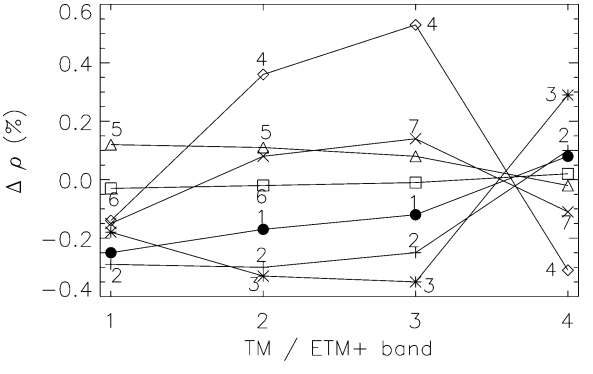

Figure 4. Reflectance difference $\Delta\rho=\bar{\rho}_{\mathrm{swir2}}-\bar{\rho}_{\mathrm{vnir}}$ for seven selected TM/ETM+ scenes.

Table 2. Comparison of AOD differences of the VNIR/SWIR2 and SWIR1/SWIR2 methods.

Scene	ΔAOD_{vnir}	ΔAOD_{swir1}
1	+0.011	+0.011
2	−0.043	−0.040
3	+0.066	+0.041
4	−0.086	−0.021
5	−0.021	0.0
6	0.0	0.0
7	−0.088	−0.042
RMS	0.056	0.028

SWIR1 versus the SWIR2 algorithm is of interest on its own. As expected, results of the SWIR1 algorithm (employing the Landsat bands 1–5, index 'swir1' in table 2) are clearly closer to the SWIR2 method than the VNIR approach.

4. Conclusion

First results of an automatic atmospheric correction method for Earth-observing VNIR sensors have been presented. For this study, Landsat-5 TM and Landsat-7 ETM + imagery were employed using only bands 1–4 to estimate the performance of the new VNIR algorithm. Results were compared with the established visible and SWIR band correlation technique using all reflective bands. The method was tested with multispectral imagery from Europe, USA, Canada and Mexico. The difference between both approaches was usually less than 0.5% in the average scene surface reflectance and standard deviation.

Similar to the VIS and SWIR band correlation method, an increased surface reflectance accuracy can be expected when the VIS and NIR band correlation coefficient is adapted to the geography and biome-dependent vegetation canopy reflectance behaviour. More detailed studies in this direction are required to fully exploit any band correlation method.

References

BERK, A., ANDERSON, G.P., ACHARYA, P.K., HOKE, M.L., CHETWYND, J.H., BERNSTEIN, L.S., SHETTLE, E.P., MATTHEW, M.W. and ADLER-GOLDEN, S.M., 2003, MODTRAN4 Version 3, Revision 1, User's Manual, Air Force Research Laboratory, Hanscom AFB, Bedford, MA, U.S.A.

BOJINSKI, S., SCHLÄPFER, D., SCHAEPMAN, M., KELLER, J. and ITTEN, K., 2004, Aerosol mapping over land with imaging spectroscopy using spectral autocorrelation. *International Journal of Remote Sensing*, **25**, pp. 5025–5047.

KALYANARAMAN, S., RAJANGAM, R.K. and RATTAN, R., 1995, Indian remote sensing spacecraft—1C/1D. *International Journal of Remote Sensing*, **16**, pp. 791–799.

KAUFMAN, Y.J., 1985, The atmospheric effect on the separability of field classes measured from satellites. *Remote Sensing of Environment*, **18**, pp. 21–34.

KAUFMAN, Y.J. and SENDRA, C., 1988, Algorithm for automatic atmospheric corrections to visible and near–IR imagery. *International Journal of Remote Sensing*, **9**, pp. 1357–1381.

KAUFMAN, Y.J., WALD, A.E., REMER, L.A., GAO, B.-C., LI, R.-R. and FLYNN, L., 1997, The MODIS 2.1 μm channel—correlation with visible reflectance for use in remote sensing of aerosol. *IEEE Transactions on Geoscience and Remote Sensing*, **35**, pp. 1286–1298.

RICHTER, R., 1996, A spatially adaptive fast atmospheric correction algorithm. *International Journal of Remote Sensing*, **17**, pp. 1201–1214.

RICHTER, R., 1998, Correction of satellite imagery over mountainous terrain. *Applied Optics*, **37**, pp. 4004–4015.

SCHLÄPFER, D., BOREL, C.C., KELLER, J. and ITTEN, K.I., 1998, Atmospheric precorrected differential absorption technique to retrieve columnar water vapor. *Remote Sensing of Environment*, **65**, pp. 353–366.